



Establishment of oxaliplatin-resistant gastric cancer organoids: importance of myoferlin in the acquisition of oxaliplatin resistance

Kenji Harada¹ · Naoya Sakamoto¹ · Shoichi Ukai¹ · Yusuke Yamamoto² · Quoc Thang Pham¹ · Daiki Taniyama¹ · Ririno Honma¹ · Ryota Maruyama¹ · Tsuyoshi Takashima¹ · Hiroshi Ota³ · Yuki Takemoto³ · Kazuaki Tanabe⁴ · Hideki Ohdan³ · Wataru Yasui¹

Received: 4 January 2021 / Accepted: 22 June 2021 / Published online: 16 July 2021
© The International Gastric Cancer Association and The Japanese Gastric Cancer Association 2021

Abstract

Background The attainment of drug resistance in gastric cancer (GC) is a problematic issue. Although many studies have shown that cancer stem cells (CSCs) play an important role in the acquisition of drug resistance, there is no clinically available biomarker for predicting oxaliplatin (L-OHP) resistance in relation to CSCs. Organoid technology, a novel 3D cell culture system, allows harboring of patient-derived cancer cells containing abundant CSCs using niche factors in a dish.

Methods In this study, we established L-OHP-resistant gastric cancer organoids (GCOs) and evaluated their gene expression profile using microarray analysis. We validated the upregulated genes in the L-OHP-resistant GCOs compared to their parental GCOs to find a gene responsible for L-OHP resistance by qRT-PCR, immunohistochemistry, in vitro, and in vivo experiments.

Results We found myoferlin (MYOF) to be a candidate gene through microarray analysis. The results from cell viability assays and qRT-PCR showed that high expression of MYOF correlated significantly with the IC₅₀ of L-OHP in GCOs. Immunohistochemistry of MYOF in GC tissue samples revealed that high expression of MYOF was significantly associated with poor prognosis, T grade, N grade, and lymphatic invasion, and showed MYOF to be an independent prognostic indicator, especially in the GC patients treated with platinum-based chemotherapy. The knockdown of MYOF repressed L-OHP resistance, cell growth, stem cell features, migration, invasion, and in vivo tumor growth.

Conclusions Our results suggest that MYOF is highly involved in L-OHP resistance and tumor progression in GC. MYOF could be a promising biomarker and therapeutic target for L-OHP-resistant GC cases.

Keywords Organoids · Oxaliplatin · Gastric cancer · MYOF

Introduction

Gastric cancer (GC) is the third leading cause of cancer death worldwide [1]. The prognosis of GC is improving due to the development of chemotherapy; however, the remaining major challenges include recurrence and acquisition of resistance to anti-cancer drugs. Oxaliplatin (L-OHP) is one of the anti-cancer drugs used as first-line treatment for GC that exerts anti-tumor effects by forming cross-links on DNA and RNA. As with other anti-cancer drugs, intrinsic or acquired resistance to L-OHP is a major clinical problem, and no biomarkers are clinically available for L-OHP response so far. Recently, cancer stem cells (CSCs) were shown to be involved in the development of drug resistance [2, 3], and elucidation of the mechanisms and biomarkers of L-OHP resistance in CSCs is urgently required. Hence,

✉ Naoya Sakamoto
naosakam@east.ncc.go.jp

¹ Department of Molecular Pathology, Graduate School of Biomedical and Health Sciences, Hiroshima University, 1-2-3 Kasumi, Minami-ku, Hiroshima 734-8551, Japan

² Division of Molecular and Cellular Medicine, National Cancer Center Research Institute, Tokyo, Japan

³ Department of Gastroenterological and Transplant Surgery, Graduate School of Biomedical and Health Sciences, Hiroshima University, Hiroshima, Japan

⁴ Department of Health Care for Adults, Graduate School of Biomedical and Health Sciences, Hiroshima University, Hiroshima, Japan

the major goal is to discover novel predictive biomarkers and overcome L-OHP resistance in GC in relation to CSCs.

In this research, we used organoids as a model of GC to focus on CSCs. Cancer organoids have been applied to various types of cancer tissue including GC [4–8], and they are well known to sustain stem cells and reflect the genetic/histological features of the parental cancer from which they are derived [9]. Therefore, we considered the gastric cancer organoid (GCO) as an ideal *in vitro* model for investigating new candidate genes responsible for L-OHP resistance with the aim of elucidating the mechanism of L-OHP resistance in gastric CSCs.

In this study, we successfully established three independent L-OHP-resistant GCOs and performed a comprehensive gene expression analysis using microarray analysis. We then combined the result with microarray data from 5-fluorouracil (5-FU)-resistant GCOs obtained in our previous study [10]. After comparing the two expression profiles, myoferlin (MYOF) was chosen as a candidate gene responsible only for L-OHP resistance and not that for 5-FU in GCOs. MYOF is a 230 kDa protein belonging to the ferlin family, which is an evolutionarily conserved family of vesicle fusion proteins [11, 12]. MYOF is reported to be involved in plasma membrane integrity, myoblast fusion, and vesicle trafficking [11, 13–15]. Recent studies have shown that MYOF is overexpressed in several human cancers and enhances tumor progression by regulating migration, invasion, and tumorigenesis [16, 17]. However, the function of MYOF in GC, and especially its effects on drug sensitivity, has received little attention.

To confirm the use of MYOF, we immunohistochemically evaluated the expression of MYOF in GC tissue samples and assessed the correlation between its expression and L-OHP-based therapeutic outcomes. Furthermore, we analyzed the effects of MYOF knockdown (KD) using both GC cell lines and GCOs.

Materials and methods

Human tissues

Human GC and normal gastric tissues were obtained from patients who underwent surgery at the Department of Gastroenterological and Transplant Surgery, Hiroshima University Hospital, and at Kure Medical Center and Chugoku Cancer Center. Tumor staging was determined according to the TNM classification system. Histological classifications were determined based on the guidelines of the Japanese Research Society for Gastric Cancer [18]. Written informed consent for the establishment of the organoids was obtained from all of the patients. This study was approved by the Ethics Committee for Human Genome Research of Hiroshima

University, Hiroshima (E-597-01), and was conducted in accordance with the Ethical Guidance for Human Genome/ Gene Research of the Japanese Government.

Establishment and culture of human GCOs

Human GC and normal gastric organoids were established and cultured in organoid media containing the niche factors as described previously [10] and were passaged twice a week with a split ratio of 1:3/1:6. Clinical data of the patient-derived organoids used in this study including the establishment of L-OHP-resistant GCOs are summarized in Supplementary Table 1. Treatment with chemotherapeutics was performed 24 h after seeding using L-OHP. The number and size of organoids with multiple buddings were counted 7 days after seeding the 5.0×10^3 cells in 50 μ L of Matrigel. Organoids were separated into single cells by Partec Cell-Trics (Sysmex, Hyogo, Japan).

Cell lines

Four cell lines derived from human GC (MKN-1, MKN-45, MKN-74, and TMK-1) were purchased from the Japanese Collection of Research Bioresources Cell Bank (Osaka, Japan). All cell lines were maintained as described previously in a humidified atmosphere of 5% CO₂ and 95% air at 37 °C [19].

qRT-PCR

RNA isolation and synthesization of complementary DNA were performed as described previously [10]. Details are described in Supplementary Materials and Methods.

MTT viability assay

Cell and organoid growth were assessed with a standard MTT assay that detects dehydrogenase activity in viable cells. The number of cells initially seeded was 2×10^3 . The cells were seeded in each well of 96-well culture plates. After 24 h, the cells were treated with various concentrations of L-OHP (Yakult, Tokyo, Japan) with/without WJ460 (MedChemExpress, NJ, USA). After another 72 h, the culture medium was removed, and 50 μ L of a 0.5 mg/mL solution of MTT (Sigma-Aldrich) was added to each well. The plates were then incubated for 1 h at 37 °C. The MTT solution was then removed and replaced with 50 μ L of dimethyl sulfoxide (Wako, Osaka, Japan) per well, and the absorbance at 540 nm was measured using an Envision 2104 Multilabel Reader (PerkinElmer, Inc., Waltham, MA, USA). Before adding DMSO, Matrigel was dissolved in 100 μ L of 2% SDS (Wako).

Immunohistochemistry and scoring

Immunohistochemical analysis was performed with a Dako Envision + Mouse/Rabbit Peroxidase Detection System (Dako Cytomation, Carpinteria, CA, USA). Antigen retrieval was performed by pressure cooker heating in citrate buffer (pH 6.0) for 5 min. Peroxidase activity was blocked with 3% H₂O₂-methanol for 10 min. Sections were incubated with a rabbit polyclonal anti-MYOF antibody (HPA014245, 1:200; Sigma-Aldrich) or mouse monoclonal anti-CD44 antibody (sc-7297, 1:50; Santa Cruz Biotechnology) for 1 h at room temperature, followed by incubation with Envision + anti-mouse or anti-rabbit peroxidase for 1 h. For color reactions, sections were incubated with DAB Substrate-Chromogen Solution (Dako Cytomation) for 5 min. Sections were counterstained with 0.1% hematoxylin. Reactions lacking a primary antibody were used as negative controls.

Two surgical pathologists (N.S. and D.T.) independently evaluated the staining without knowledge of the clinical and pathological parameters or patient outcome. Inter-observer differences were resolved by consensus review at a double-headed microscope after independent reviews.

Microarray

Details are described in Supplementary Materials and Methods [10].

Western blot

Cells were lysed as described previously [20]. Details are described in Supplementary Materials and Methods.

Generation of MYOF KD GC cell lines

Lentivirus was packaged as described previously [21]. Details are described in Supplementary Materials and Methods.

Generation of MYOF KD GCOs

Lentivirus was packaged as described previously [21]. Details are described in Supplementary Materials and Methods.

Spheroid colony formation

Details are described in Supplementary Materials and Methods.

Migration assay

To evaluate cell motility, a wound-healing assay was performed as described previously [22]. Details are described in Supplementary Materials and Methods.

Invasion assay

Modified Boyden chamber assays were carried out as described previously [23]. Details are described in Supplementary Materials and Methods.

Xenograft tumor mouse models

Details are described in Supplementary Materials and Methods. All animal care in our laboratory was in accordance with the guidelines for animal and recombinant DNA experiments of Hiroshima University (Hiroshima, Japan, A21-54-2).

Statistical analysis

Statistical differences were evaluated by Student *t* test or Mann–Whitney *U* test as appropriate. The correlation between expression levels of MYOF and clinicopathological characteristics was analyzed with Fisher's exact test. The results are expressed as the mean \pm standard deviation of triplicate measurements. We considered $p < 0.05$ to be statistically significant.

Results

Establishment of L-OHP-resistant GCOs

To approach L-OHP resistance in gastric CSCs, we tried to establish L-OHP-resistant GCOs. By adding increasing doses of L-OHP in the culture medium over time, we successfully established three independent L-OHP-resistant GCOs (Fig. 1a). The concentration of L-OHP was increased until it reached more than twice the parental IC₅₀ values. The IC₅₀ values of the parental GCOs and newly established L-OHP-resistant GCOs were measured by an organoid viability assay (Fig. 1b). We confirmed that each of the L-OHP-resistant GCOs had IC₅₀ values 3.2–7.3-fold higher than that of the parental GCOs. The morphology of GCOs was observed under a microscope to determine that all three L-OHP-resistant GCOs exhibited more crypt-like

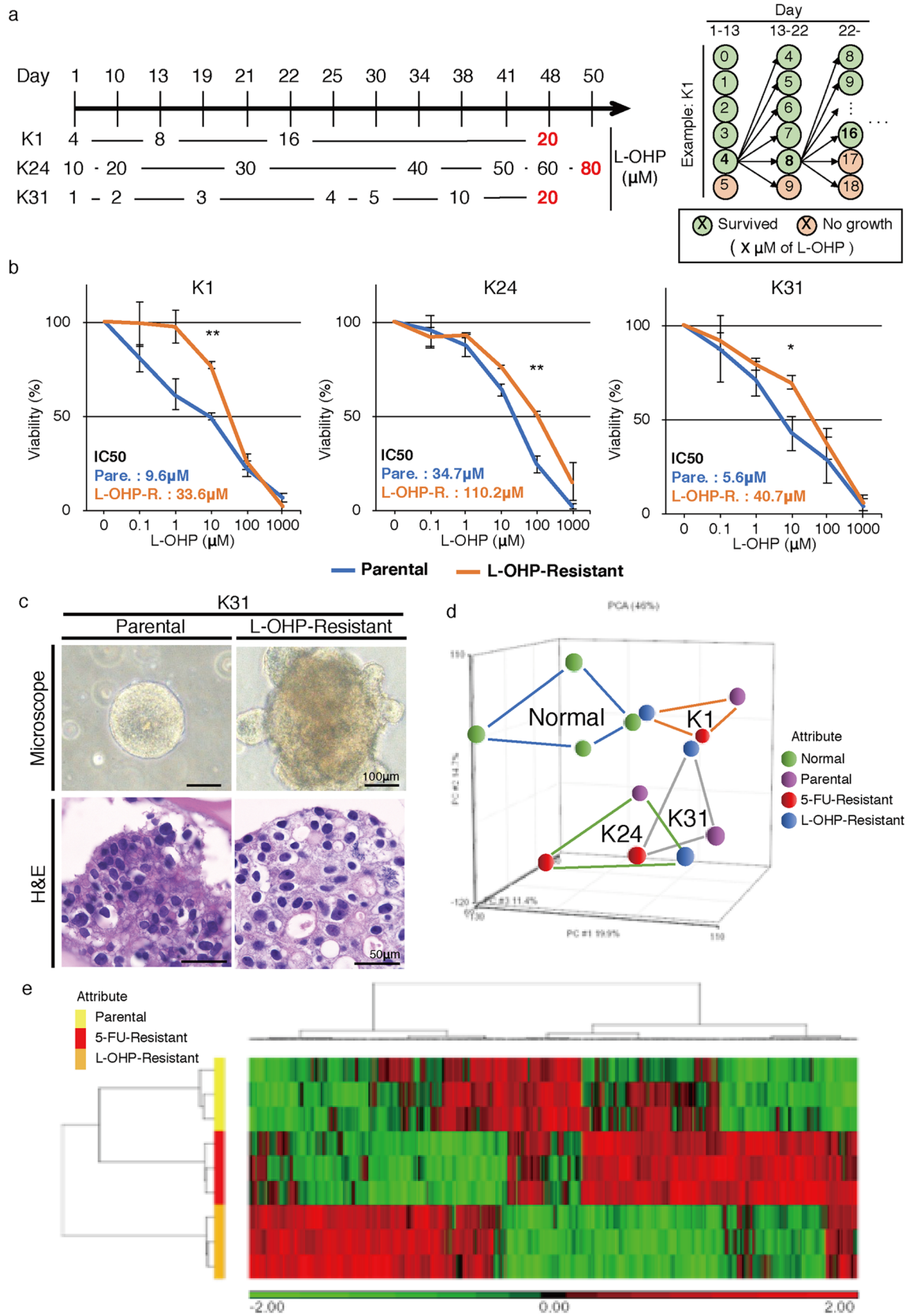


Fig. 1 Establishment and microarray analysis of L-OHP-resistant GCOs. **a** L-OHP administration timeline and its schema. Three different GCOs (K1, K24, and K31) established from three GC patients were used. Each organoid line was treated with multiple concentrations of L-OHP on the same day. The GCO that tolerated the highest concentration of L-OHP was passaged after becoming confluent. The concentration of L-OHP was gradually increased after each passaging. **b** Dose-response curves of the parental and L-OHP-resistant GCOs to L-OHP assessed by MTT assay. GCOs were cultured with several concentrations of L-OHP for 72 h. Error bars represent s.d. * $p < 0.05$ by Student *t* test. ** $p < 0.01$ by Student *t* test. **c** Representative image of morphology assessed under phase-contrast microscopy and H and E staining. Original magnification $\times 100, \times 1000$, respectively. **d** The principal component analysis (PCA) plot generated from microarray analysis. Each dot represents individual organoids. Dots are colored by the status of the organoids (green: normal gastric organoid, purple: parental GCO, red: 5-FU-resistant GCO, blue: L-OHP-resistant GCO). **e** The heatmap of the variance of gene expression profiles (ANOVA $p < 0.01$) generated from microarray analysis. Each row represents the status of GCOs (Parental, 5-FU-resistant, and L-OHP-resistant)

morphology called budding (Fig. 1c, Supplementary Fig. 1a). The H and E staining revealed that the L-OHP-resistant GCOs displayed clear round nucleoli (Fig. 1c, Supplementary Fig. 1a). These two consistent changes in morphology and H and E staining among GCOs showed that they closely resembled the known morphological features of CSCs [24]. Furthermore, we confirmed that the expression of CD44, a well-known CSC marker for GC, was significantly upregulated at both mRNA and protein levels in L-OHP-resistant GCOs than its parental (Supplementary Fig. 1b, c), supporting the increasing proportion of CSCs in L-OHP-resistant GCOs. Additionally, we performed qRT-PCR on each exon of CD44. We found that most of CD44 exons were, on the whole, upregulated; we did not detect upregulation of the specific CD44 exon variant (data not shown).

We also established three L-OHP-resistant GC cell lines, which took much longer to establish compared to the GCOs (Supplementary Fig. 2a). The IC₅₀ values of each parental and L-OHP-resistant GC cell line are shown in Supplementary Fig. 2b. Interestingly, there were no remarkable morphological changes in common to all L-OHP-resistant GC cell lines in the microscopic and H and E stain observations (Supplementary Fig. 2c, d).

Microarray analysis of L-OHP-resistant GCOs

We then performed a microarray analysis to identify molecules that show alteration of specific expression by comparing the variances and differences in the expression profiles between the GCO samples. The gene expression data from this study and our previous study (GSE154127), which elucidated 5-FU-resistant GCOs, were combined and analyzed together. The results of the principal component analysis

showed that every single pair of parental, 5-FU-resistant, and L-OHP-resistant GCOs were closely mapped (Fig. 1d). However, the normal gastric organoids were plotted in a different cluster (Fig. 1d). By considering the variance of gene expression profiles, we found that there were 548 genes expressed differently between the parental, 5-FU-resistant, and L-OHP-resistant GCOs (ANOVA $p < 0.01$) (Fig. 1e, Supplementary Table 2). Interestingly, among these 548 genes, only a few were working in common with 5-FU and L-OHP-resistant GCOs. These findings suggest that GCOs acquire resistance to 5-FU and L-OHP in a different manner.

Detection of MYOF and its validation by qRT-PCR and in silico analyses

Through comparison of the expression profiles between normal gastric organoids and the parental, 5-FU-resistant, and L-OHP-resistant GCOs, we found 389 upregulated genes and 747 downregulated genes specifically in the L-OHP-resistant GCOs (> 1.5 fold change, $p < 0.05$) (Fig. 2a). All of the genes on the Venn diagram are listed in Supplementary Table 3–8. We performed pathway enrichment analysis on these genes but could not find any pathway that was up- or down-regulated (data not shown). Interestingly, there were only 23 upregulated and 48 downregulated genes in which the expression changed in both 5-FU and L-OHP-resistant GCOs. To specifically identify an ideal biomarker for L-OHP resistance, we decided to focus on 366 genes that were upregulated only in the L-OHP-resistant GCOs. We list the top five protein-coding genes from these 366 genes in Supplementary Table 9. Among these five genes, AKR1B10 has already been reported in gastric cancer, and AKR1B15 was highly homologous to AKR1B10. We performed qRT-PCR to examine the expression levels of PPP3CC, ANKDD1B, and MYOF in the parental and L-OHP-resistant GCOs and elucidated that only MYOF showed significantly higher expression levels in the L-OHP-resistant GCOs (Fig. 2b), while expression levels of PPP3CC and ANKDD1B were quite low in the GCOs (data not shown). Interestingly, the expression levels of MYOF were not changed in the L-OHP-resistant GC cell lines that hold fewer CSCs compared to organoids, indicating that MYOF is upregulated mainly in L-OHP-resistant CSCs (Fig. 2c). Accordingly, we decided to focus on MYOF as a candidate for a novel biomarker in L-OHP gastric CSCs. Further, we performed qRT-PCR for MYOF in GCOs revealing that MYOF is upregulated in GCOs compared to corresponding normal gastric organoids (Supplementary Fig. 3). A strong correlation between the IC₅₀ values of L-OHP and the expression levels of mRNA MYOF was also detected (Fig. 2d). Therefore, these data suggest that MYOF could be a potential candidate as a biomarker that reflects L-OHP resistance in GC.

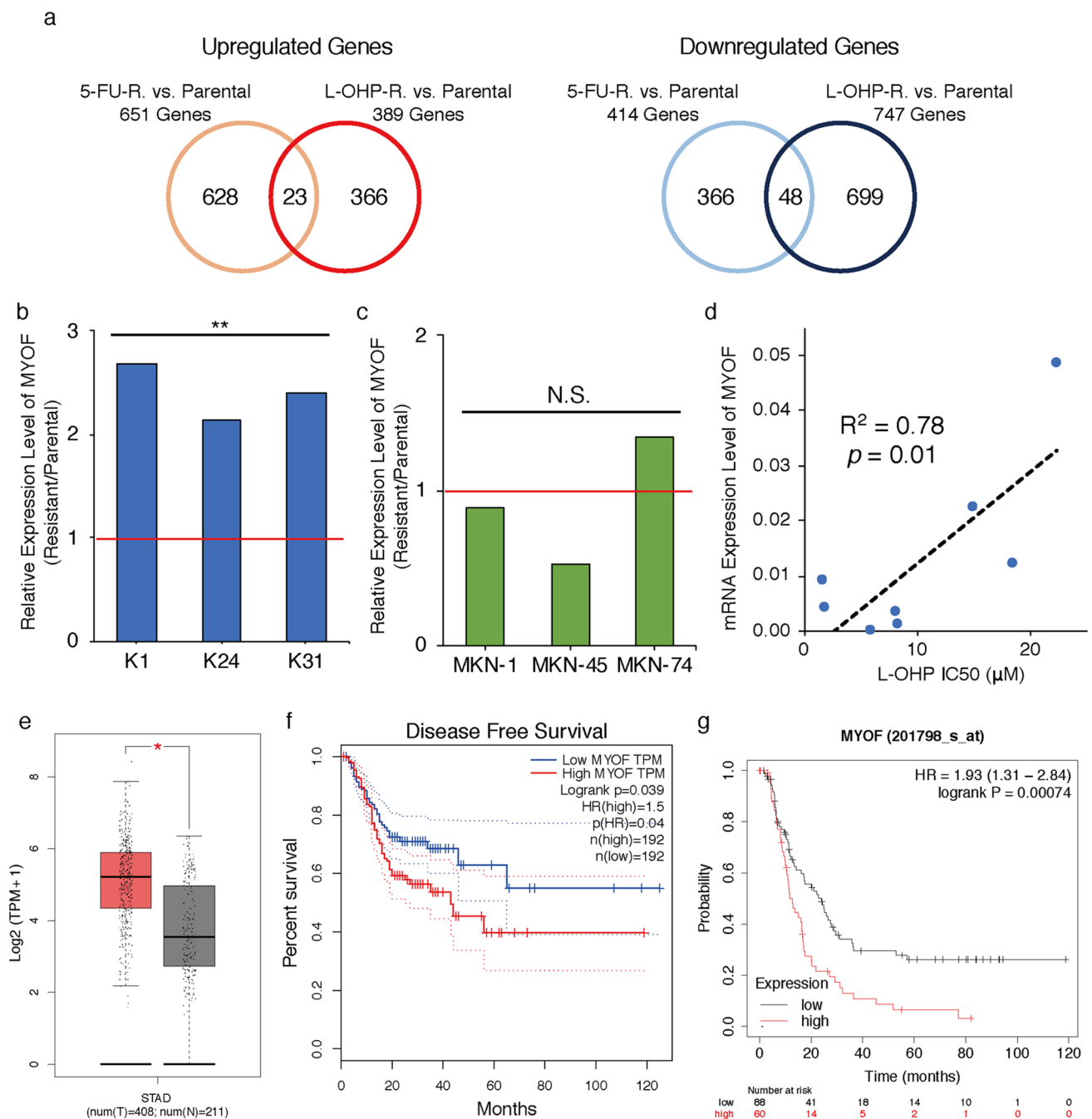


Fig. 2 Detection and validation of MYOF by qRT-PCR and in silico analyses. **a** Venn diagrams of upregulated and downregulated genes (>1.5 fold change, $p < 0.05$) in either 5-FU-resistant or L-OHP-resistant GCOs by microarray analysis. Numbers in the diagram show the total number of genes in the section. **b** Relative mRNA expression level of MYOF in GCOs evaluated by qRT-PCR. Fold changes of each resistant GCO over parental GCO were shown. $**p < 0.01$ by Student t test. **c** Relative mRNA expression level of MYOF in GC cell lines evaluated by qRT-PCR. Fold changes of each resistant GC cell line over the parental GC cell line were shown. N.S. represents non-significant change. **d** Relationship between the IC50 values

of L-OHP and the mRNA expression level of MYOF in 8 different GCOs. $p = 0.01$ by Mann-Whitney U test. **e** MYOF expression profile in the TCGA-STAD dataset and GTEx dataset. The image was taken from the GEPIA (Gene Expression Profiling Interactive Analysis) online database (<http://gepia.cancer-pku.cn>). T (red), tumor; N (gray), normal. $*p < 0.01$. **f** Disease-free survival of patients with differences in MYOF expression level. GEPIA online database was used for the analysis. $p < 0.05$ by log-rank test. **g** Kaplan-Meier curves of overall survival in patients with stage 4 GC. The Kaplan-Meier Plotter database (www.kmplot.com) was used for the analysis. $p < 0.01$ by log-rank test

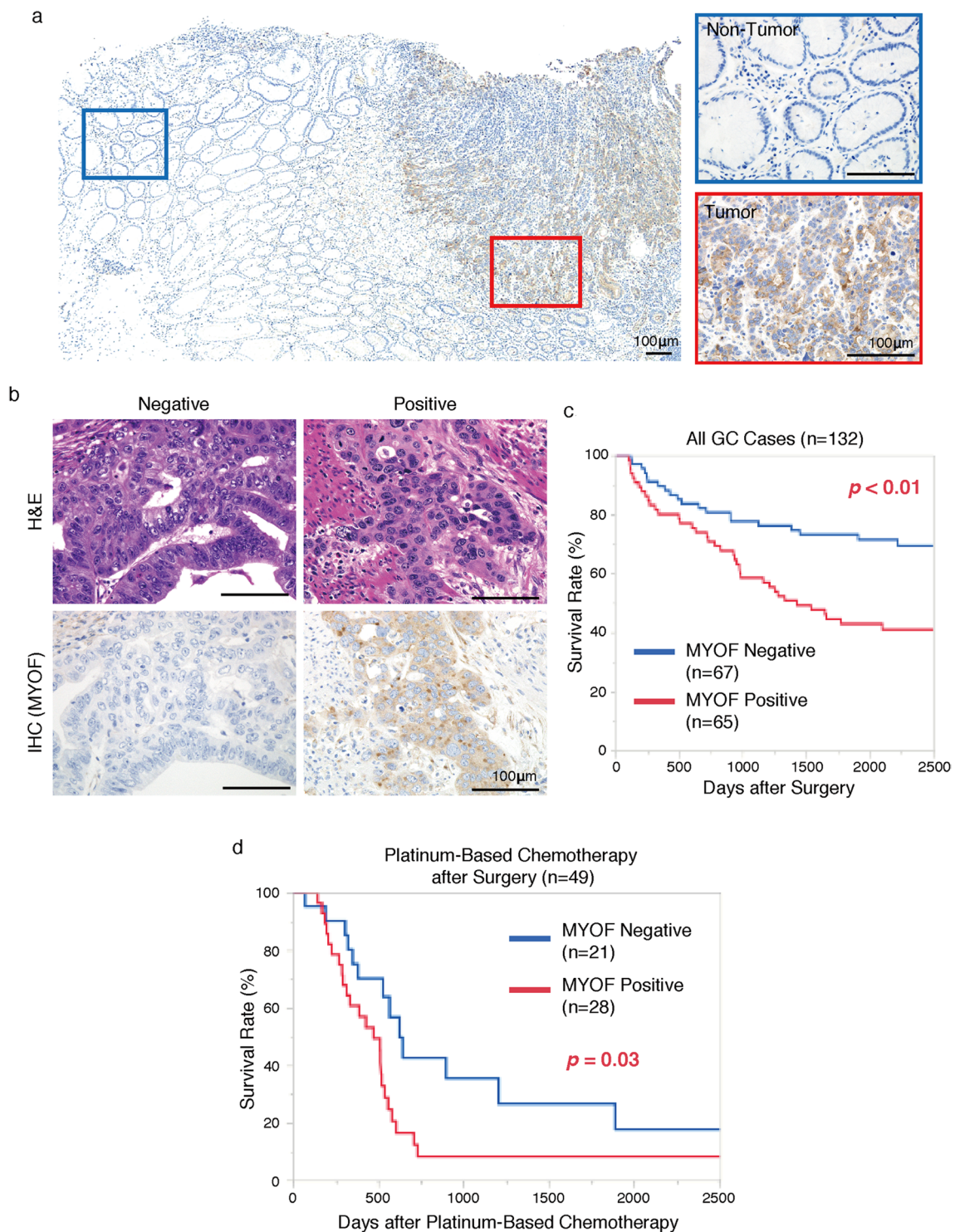


Fig. 3 Immunohistochemistry and Kaplan–Meier analyses for MYOF in human gastric tissues. **a** Representative image of immunohistochemical staining of MYOF in GC tissue samples. Original magnification $\times 40$ (left) and $\times 1000$ (right). **b** Representative H and E and immunohistochemical staining images of MYOF-positive and negative cases. Original magnification $\times 1000$. **c** Survival curves by the

difference in MYOF expression in 132 GC samples. Red, MYOF positive cases (65 cases); Blue, MYOF negative cases (67 cases). $p < 0.01$ by log-rank test. **d** Survival curves by MYOF expression in GC tissue samples from patients with a history of platinum-based therapy. Red, MYOF positive cases (28 cases); Blue, MYOF negative cases (21 cases). $p = 0.03$ by log-rank test

Moreover, we analyzed the correlation between the expression levels of MYOF and prognosis in the TCGA-STAD database and GTEx database containing 408 GC and 211 normal gastric samples in total (Gene Expression Profiling Interactive Analysis, GEPIA; <http://gepia.cancer-pku.cn/>). We determined that MYOF was overexpressed in tumor tissues compared to normal tissues (Fig. 2e) and that the higher expression levels of MYOF in GC tissue were associated with a worse prognosis (Fig. 2f). Interestingly, MYOF expression level correlated with CD44, β -catenin, vimentin, and cyclin D1 expression, well-known genes related to CSC/epithelial-mesenchymal transition (EMT) (Supplementary Fig. 4). We also used a different online database, Kaplan–Meier plotter (www.kmplot.com), to verify the association between MYOF expression and prognosis. Similar to the TCGA data (Fig. 2f), we confirmed a significant correlation between MYOF expression and poor clinical outcome in stage 4 GC patients (Fig. 2g). These results further support that MYOF may potentially be a predictive marker for GC patients.

MYOF was significantly associated with poor clinical outcome and invasion in GC patients

We performed immunohistochemistry for MYOF using three pairs of the normal gastric organoids, parental GCOs, and L-OHP-resistant GCOs. All the normal organoids and K1 and K31 GCOs were not or only slightly stained, while K24 GCO and all L-OHP-resistant GCOs showed strong granule-like stains in the cytoplasm (Supplementary Fig. 5). K24 L-OHP-resistant GCO also showed strong membrane staining (Supplementary Fig. 5). Next, we performed immunohistochemistry on specimens from 132 surgically resected GC cases to clarify the clinical impact of MYOF in GC. Strong cytoplasmic and/or membrane staining was detected in cancer cells, whereas stromal cells and non-cancerous epithelial cells were either not or only slightly stained (Fig. 3a, Supplementary Fig. 6a, b). Immunostaining was considered positive for MYOF when a membranous stain and/or a granule-like stain in the cytoplasm was observed in more than 5% of tumor cells (Fig. 3b, Supplementary Fig. 6a). In total, 65 (49%) of the 132 GC cases were positive for MYOF. The correlations between MYOF expression and clinicopathological characteristics were analyzed, and significant correlations were detected between MYOF expression and T grade, N grade, and lymphatic invasion (Table 1).

We next examined the relationship between survival probability and MYOF expression in the 132 GC cases using Kaplan–Meier analysis. The survival curve showed significantly poorer survival in the MYOF-positive GC cases (Fig. 3c). The 5 year overall survival rates were 73.3% and 42.9% for MYOF-negative and -positive cases, respectively. The association between MYOF expression and mortality

was also evaluated by univariate and multivariate Cox proportional hazards analyses. Univariate analysis showed age, T grade, N grade, M grade, lymphatic invasion, vascular invasion, TNM stage, and MYOF expression to be associated with survival, whereas multivariate analysis showed MYOF expression to be an independent prognostic indicator as were M grade, lymphatic invasion, and TNM stage (Table 2).

Because we chose MYOF as a candidate gene responsible for L-OHP resistance, we further investigated the association between its expression and clinical outcome in the 49 GC patients who had received platinum-based chemotherapy, including L-OHP. In contrast to the previous analysis of clinicopathological characteristics (Table 1), there was no significant correlation between MYOF and clinicopathological characteristics in this cohort (Supplementary Table 10). Nevertheless, the survival curve showed significantly poorer outcomes in the MYOF-positive GC cases (Fig. 3d), and

Table 1 Relationship between MYOF expression and clinicopathological characteristics in 132 GC cases

| Factor | MYOF expression | | <i>p</i> value |
|------------------------------------|-----------------|----------|----------------|
| | Positive | Negative | |
| Age (years) | | | |
| < 65 (<i>n</i> = 39) | 14 | 25 | 0.046 |
| ≥ 65 (<i>n</i> = 93) | 51 | 42 | |
| Sex | | | |
| Male (<i>n</i> = 100) | 46 | 54 | 0.187 |
| Female (<i>n</i> = 32) | 19 | 13 | |
| Differentiation | | | |
| Differentiated (<i>n</i> = 57) | 30 | 27 | 0.497 |
| Un-differentiated (<i>n</i> = 75) | 35 | 40 | |
| T grade | | | |
| T0/T1/T2 (<i>n</i> = 63) | 22 | 41 | 0.002 |
| T3/T4 (<i>n</i> = 69) | 43 | 26 | |
| N grade | | | |
| N0 (<i>n</i> = 63) | 25 | 38 | 0.035 |
| N1/N2/N3 (<i>n</i> = 69) | 40 | 29 | |
| M grade | | | |
| M0 (<i>n</i> = 125) | 60 | 65 | 0.253 |
| M1 (<i>n</i> = 7) | 5 | 2 | |
| Lymphatic invasion | | | |
| ly0 (<i>n</i> = 52) | 18 | 34 | 0.006 |
| ly1/2/3 (<i>n</i> = 80) | 47 | 33 | |
| Vascular invasion | | | |
| v0 (<i>n</i> = 78) | 33 | 45 | 0.055 |
| v1/2/3 (<i>n</i> = 54) | 32 | 22 | |
| Stage | | | |
| Stage 0/I/II (<i>n</i> = 87) | 39 | 48 | 0.158 |
| Stage III/IV (<i>n</i> = 45) | 26 | 19 | |

Bold values indicate *p* < 0.05

in the univariate and multivariate analyses, MYOF expression was an independent prognostic indicator in the patients administered platinum-based chemotherapy (Supplementary Table 11). Taken together, these data suggest that MYOF expression may be a promising biomarker for GC patients, notably for GC patients who will receive platinum-based therapy after surgery.

MYOF KD in GC cell lines enhanced L-OHP sensitivity while reducing cell growth, sphere formation, migration, and invasion

To investigate the biological functions of MYOF in GC, we first examined the protein expression levels of MYOF in four GC cell lines. MKN-1 and MKN-45 were chosen

for the KD experiments as they strongly expressed MYOF (Fig. 4a). We stably knocked down MYOF in these GC cell lines using three different shRNAs (KD#1–3) that specifically target MYOF. MYOF KD was confirmed by Western blotting (Fig. 4b, c).

We then performed a cell viability assay and confirmed that three MYOF KD GC cells showed significantly lower IC50 values than the negative control (N.C.) in both the MKN-1 and MKN-45 cell lines (Fig. 4d, e). Cell growth assay results showed that O.D. 595 values of MYOF KD cell lines differed significantly on day 4, suggesting that the proliferative capacity was reduced by MYOF KD (Fig. 4f, g). Considering the effect of altered cell proliferative capacity on drug sensitivity, we performed the cell viability assay with different initial cell numbers; however, we found that

Table 2 Univariate and multivariate Cox regression analyses of factors influencing overall survival in 132 GC cases

| Factor | Univariate analysis | | | Multivariate analysis | | |
|--------------------|---------------------|----------------|-------------------|-----------------------|----------------|----------------|
| | HR | 95% CI | <i>p</i> value | HR | 95% CI | <i>p</i> value |
| Age (years) | | | | | | |
| < 65 | 1 (Ref.) | | < 0.001 | | | |
| ≥ 65 | 4.033 | (1.955–9.757) | | | | |
| Sex | | | | | | |
| Male | 1 (Ref.) | | 0.361 | | | |
| Female | 0.764 | (0.442–1.381) | | | | |
| Differentiation | | | | | | |
| Differentiated | 1 (Ref.) | | 0.987 | | | |
| Undifferentiated | 1.000 | (0.600–1.699) | | | | |
| T grade | | | | | | |
| T0/T1/T2 | 1 (Ref.) | | < 0.001 | 1 (Ref.) | | 0.954 |
| T3/T4 | 3.320 | (1.903–6.089) | | 1.024 | (0.455–2.308) | |
| N grade | | | | | | |
| N0 | 1 (Ref.) | | < 0.001 | 1 (Ref.) | | 0.355 |
| N1/N2/N3 | 4.241 | (2.379–8.047) | | 1.467 | (0.652–3.302) | |
| M grade | | | | | | |
| M0 | 1 (Ref.) | | < 0.001 | 1 (Ref.) | | 0.003 |
| M1 | 10.089 | (3.998–22.261) | | 4.519 | (1.889–10.813) | |
| Lymphatic invasion | | | | | | |
| ly0 | 1 (Ref.) | | < 0.001 | 1 (Ref.) | | 0.019 |
| ly1/2/3 | 4.944 | (2.542–10.802) | | 2.447 | (1.107–5.412) | |
| Vascular invasion | | | | | | |
| v0 | 1 (Ref.) | | 0.002 | 1 (Ref.) | | 0.684 |
| v1/2/3 | 2.291 | (1.367–3.877) | | 0.879 | (0.473–1.634) | |
| Stage | | | | | | |
| Stage 0/II/III | 1 (Ref.) | | < 0.001 | 1 (Ref.) | | 0.022 |
| Stage III/IV | 4.763 | (2.824–8.161) | | 2.451 | (1.107–5.428) | |
| MYOF expression | | | | | | |
| Negative | 1 (Ref.) | | 0.001 | 1 (Ref.) | | 0.017 |
| Positive | 2.362 | (1.389–4.142) | | 1.957 | (1.112–3.447) | |

HR hazard ratio, CI confidence interval, Ref. Reference

Bold values indicate $p < 0.05$

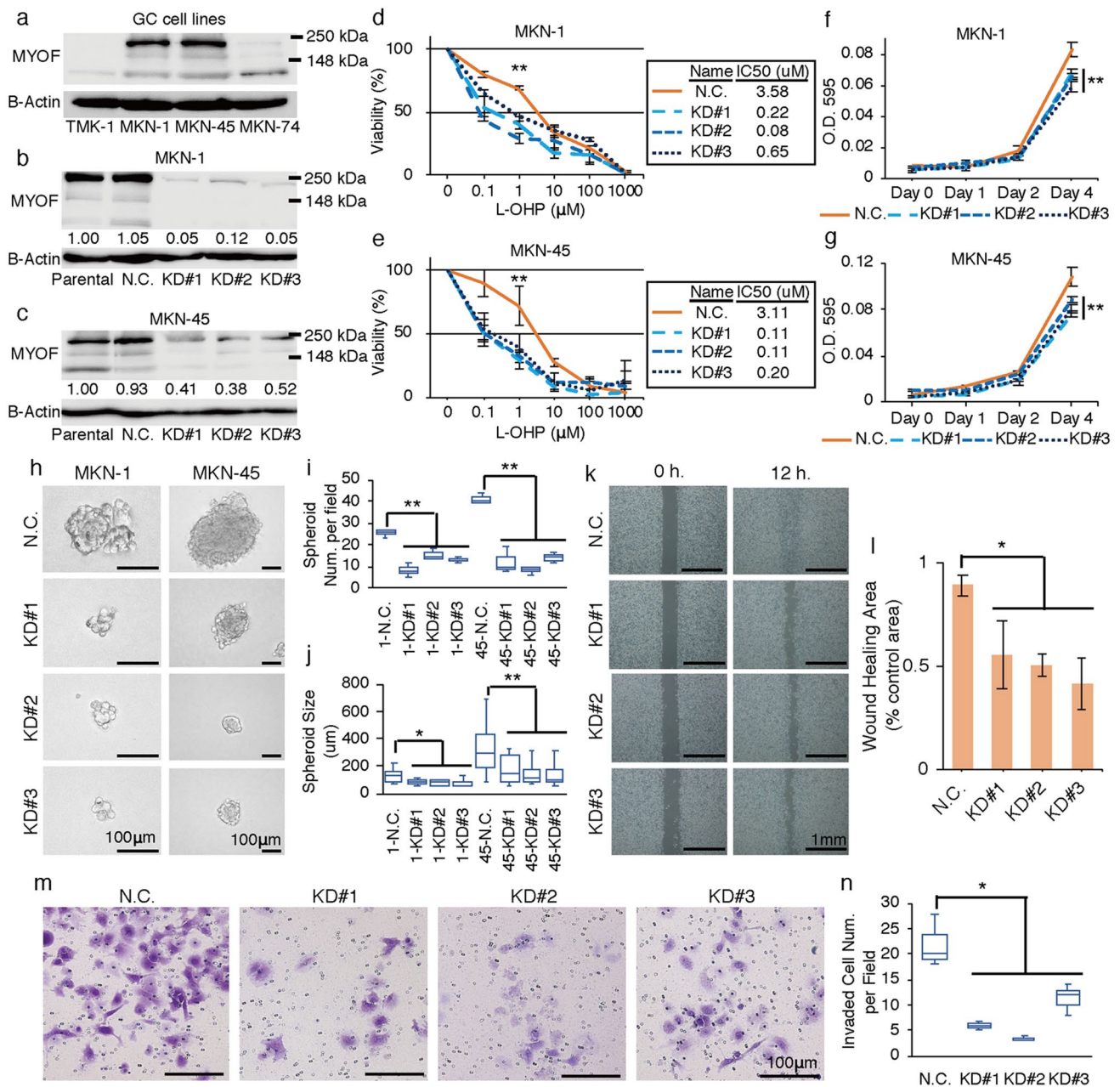


Fig. 4 MYOF knockdown (KD) in GC cell lines enhances L-OHP sensitivity while reducing cell growth, sphere formation, migration, and invasion. **a** The expression levels of MYOF protein in GC cell lines (TMK-1, MKN-1, MKN-45, and MKN-74) by Western blotting. **b, c** Western blot analysis detecting parental, negative control (N.C.; non-silencing shRNA), and efficient KD of MYOF (KD#1–3; three different shRNAs targeting MYOF) in MKN-1 and MKN-45, respectively. Relative protein expression levels compared to the parental expression are shown in the figure. **d, e** Dose-response curves of MKN-1 and MKN-45 cells transduced with N.C. and KD#1–3 vectors assessed by MTT assay. Each cell lines were cultured with various concentrations of L-OHP for 72 h. Error bars represent s.d. ** $p < 0.01$ by Student *t*-test. **f, g** Cell growth of MKN-1 and MKN-45 cells assessed by MTT assay. O.D. 595 values were analyzed on day 0, 1, 2, and 4. Error bars represent s.d. ** $p < 0.01$ by Student *t* test. **h** Representative phase-contrast microscopy images of spheroids derived from MKN-1 and MKN-45 cells transduced with N.C. and KD#1–3 vectors. The spheroids were observed 7 days after seeding the equal numbers of GC cells. **i** Quantification of spheroids from the experiment described in **h**. ** $p < 0.01$ by Student *t* test. **j** Diameter of spheroids from the experiment described in **h**. * $p < 0.05$ by Student *t* test. ** $p < 0.01$ by Student *t* test. **k** Representative phase-contrast microscopy images of the wound-healing assay of MKN-1 cells transduced with N.C. and KD#1–3 vectors. The cells were scraped with the sharp end of a pipette tip to generate a cell-free area. Observed every 12 h. **l** Quantification of the wound-healing area from the experiment described in **k**. The wound-healing area was determined by the rate of cell moving towards the scratched area over time using ImageJ software. Error bars represent s.d. * $p < 0.05$ by Student *t* test. **m** Representative images of the invasion assay of MKN-1 cells transduced with N.C. and KD#1–3 vectors. Cells were passaged on Matrigel-coated culture inserts and cultured for 48 h. Cells adhering to the underside of the inserts were stained and counted. **n** Cell counts in the invasion assay described in **m**. * $p < 0.05$ by Student *t* test

the number of cells did not affect the drug sensitivity assay (Supplementary Fig. 7).

Next, we performed a spheroid formation assay to verify the effect of MYOF KD on this stem cell-like feature. The results showed a significant reduction in the number and size of the spheroids generated in the KD cells, indicating that KD of MYOF impaired CSC features (Fig. 4h–j). Furthermore, we conducted a migration and an invasion assay because we observed significant correlations between MYOF expression and the clinicopathological factors that characterize tumor migration and invasion in human GC tissues (Table 1). In the wound-healing migration assay, the MYOF KD cells showed a significant decrease in wound-healing area, indicating that KD of MYOF inhibited cell motility (Fig. 4k, l). As with the migration assay, the invasion assay also showed that MYOF KD reduced the number of cells invaded (Fig. 4m, n). These results support MYOF involvement in L-OHP resistance and also suggest that MYOF may play an important role in tumor progression, migration, and invasion.

MYOF KD in L-OHP-resistant GCOs reversed resistance and reduced organoid formation ability

Because we determined MYOF to be a candidate gene in L-OHP-resistant GCOs, we also performed KD experiments in GCOs. We used K1 and K24 L-OHP-resistant GCOs for KD of MYOF. We successfully established three independent KD GCOs and confirmed the efficiency of KD by Western blotting (Fig. 5a, b). In an organoid viability assay, MYOF KD GCOs showed significantly lower IC₅₀ values compared to the N.C. (Fig. 5c, d). We also performed an organoid formation assay and confirmed significant inhibition in the number and size of the organoids by MYOF KD (Fig. 5e–j). In addition, the MYOF inhibitor (WJ460) was applied for K1 and K24 L-OHP-resistant GCOs, confirming reduced L-OHP resistance and organoid formation ability (Supplementary Fig. 8a–h), which is consistent results to the MYOF KD GCOs (Fig. 5c–j). As a control, we found that administration of WJ460 did not alter L-OHP sensitivity in MYOF KD K1 L-OHP-resistant GCO (KD#3) and TMK-1, which have quite low expressions of MYOF (Supplementary Fig. 8i–j, Fig. 4a). These findings support the idea that L-OHP sensitivity was regulated by inhibiting MYOF. Taken together with the result of the spheroid assay of GC cell lines, these data support that MYOF promotes L-OHP resistance and CSC features in GC.

MYOF KD inhibited *in vivo* tumor growth

To further evaluate the importance of MYOF on tumor growth *in vivo*, MKN-45 MYOF KD#2 cells and their

negative controls (N.C.) were injected subcutaneously into NOD Rag Gamma (NRG) mice. As a result, although tumor weight showed a non-significant decreasing trend by MYOF KD ($p = 0.050$), tumor size and volume exhibited a significant decrease (Fig. 5k–n). These results are consistent with the *in vitro* results, strongly supporting that MYOF KD triggered a decrease in tumor growth.

Discussion

In this study, we successfully established L-OHP-resistant GCOs, and subsequent experiments revealed that MYOF may be a promising marker gene with a pivotal role in the acquisition of resistance against L-OHP in GCOs. We also observed morphological changes relating to CSCs features after L-OHP treatment, indicating that GCOs acquired L-OHP resistance. Although several studies have recently identified the genes involved in L-OHP resistance by using GC cell lines [25, 26], none of the studies, to our knowledge, have conducted comprehensive analyses aiming to elucidate the mechanism of acquisition of resistance to DNA-damaging anti-cancer drugs using cancer organoids. Our work is the first to report MYOF as a candidate biomarker for L-OHP resistance in GC using drug-resistant cancer organoids, which has never been mentioned in the studies using existing experimental models such as cell lines and animal models. From these viewpoints, our current results highlighted the effectiveness of L-OHP-resistant GCOs to examine the mechanism of L-OHP resistance in CSCs.

Our results highlight the correlation of MYOF expression with higher T and N grades, lymphatic invasion, and poorer outcomes in GC patients. Furthermore, we clarified that MYOF expression was an independent prognostic indicator in GC. In particular, high expression of MYOF predicted worse survival in patients who received platinum-based chemotherapy. We also determined that MYOF KD leads to the suppression of cell growth, sphere/organoid formation, migration, and invasion. Recent studies on breast cancer have reported a correlation between overexpression of MYOF and tumor progression, invasiveness, and EMT [17, 27]. It is well known that in the process of EMT, cancer cells extent their invasiveness, tumor-initiation ability, and drug resistance [3]. Similar to the breast cancer studies, the relationship between MYOF and worse clinical outcomes and invasiveness was also shown in melanoma [28], indicating that MYOF expression is crucial for tumor progression in various types of cancer. In the TCGA-STAD dataset, we found that MYOF expression correlated significantly with several stem cell-related markers (Supplementary Fig. 4). Several lines of study have shown that cancer cells with EMT-like features somehow possess the characteristics of CSCs [3], indicating a possible correlation between MYOF

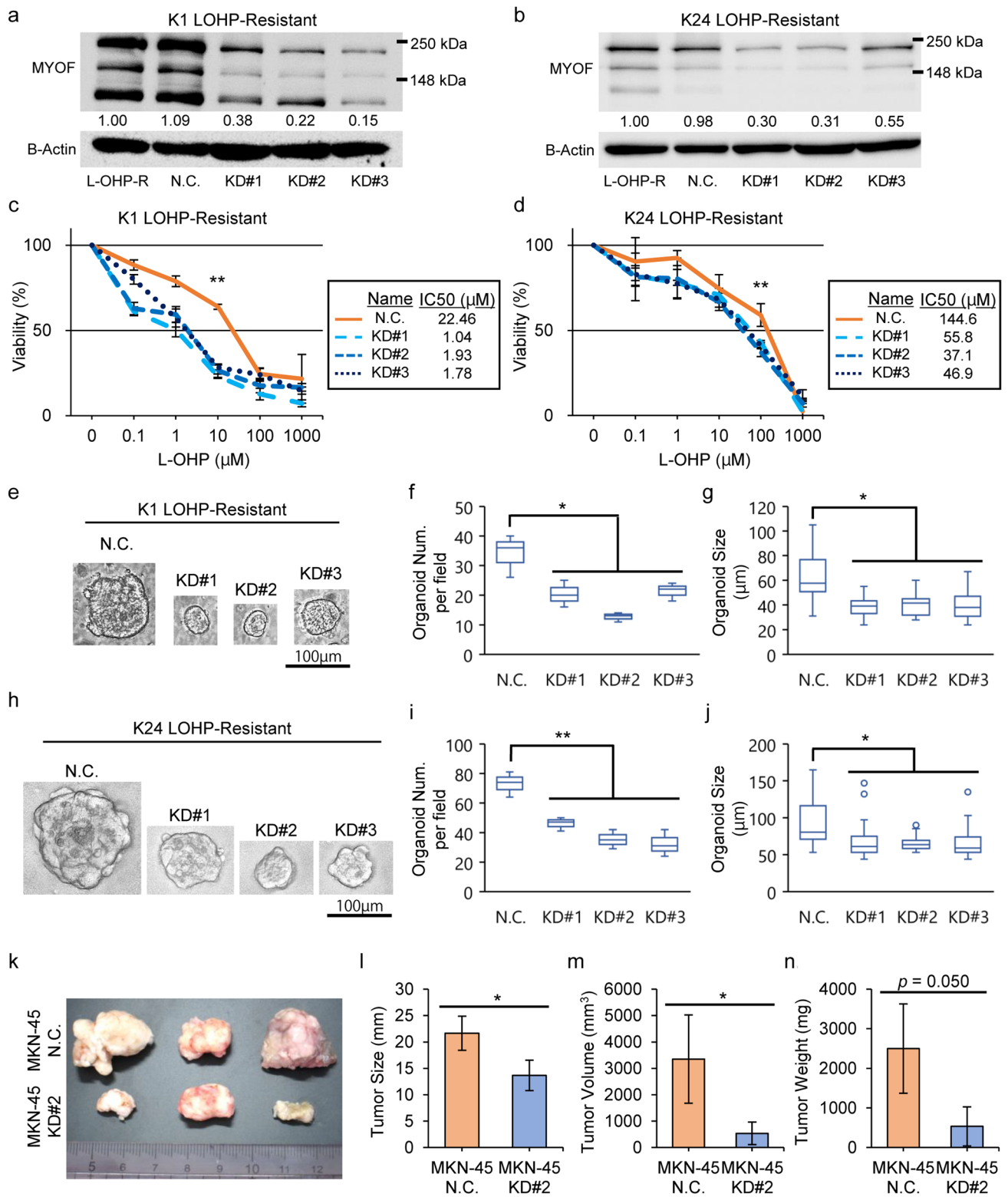


Fig. 5 MYOF knockdown (KD) in L-OHP-resistant GCOs reversed L-OHP resistance and reduced organoid formation ability. **a, b** Western blot analysis detecting MYOF protein in the L-OHP-resistant (L-OHP-R), negative control (N.C.), and efficient KD of MYOF in KD#1–3 L-OHP-resistant GCOs. Relative protein expression levels compared to the parental expression are shown in the figure. **c, d** Dose-response curves of L-OHP-resistant GCOs transduced with N.C. and KD#1–3 assessed by MTT assay. Each GCOs were cultured with several concentrations of L-OHP for 72 h. Error bars represent s.d. $**p < 0.01$ by Student *t* test. **e** Representative phase-contrast microscopy images of K1 L-OHP-resistant GCOs transduced with N.C. and KD#1–3 grown in Matrigel. The organoids were observed 7 days after passaging the equal numbers of organoid cells in 50 μ L of Matrigel. **f** Quantification of organoid from the experiment described in **e**. $*p < 0.05$ by Student *t* test. **g** Diameter of organoids from the experiment described in **e**. $*p < 0.05$ by Student *t* test. **h** Representative phase-contrast microscopy images of K24 L-OHP-resistant GCOs transduced with N.C. and KD#1–3 grown in Matrigel. The organoids were observed 7 days after seeding the equal numbers of organoid cells in 50 μ L of Matrigel. **i** Quantification of organoid from the experiment described in **h**. $**p < 0.01$ by Student *t* test. **j** Diameter of organoids from the experiment described in **h**. $*p < 0.05$ by Student *t* test. **k** Picture of tumors from mice injected with MKN-45 transfected with N.C. (upper) or KD#2 (lower). **l** Tumor major axis was measured as tumor size. $*p < 0.05$ by Student *t* test. **m** Tumor volume was calculated from major and minor axis of the tumor. $*p < 0.05$ by Student *t* test. **n** Tumor weight was measured. $p = 0.050$ by Student *t* test

and EMT. Taken together, our results suggest that MYOF may also play a crucial role in GC progression especially through its involvement in EMT, which could potentially provide insights into further detailed molecular mechanisms of how MYOF contributes to cancer progression.

Among the current first-line regimens against unresectable or recurrent GC, L-OHP is used in combination with 5-FU, but many patients acquire resistance to L-OHP [29]. In the present study, we determined that L-OHP-resistant GCOs had different gene expression profiles compared to those of 5-FU-resistant GCOs, suggesting that cancer cells change their response based on differences in the mechanism of action of anti-cancer agents. This explanation enforces the vital need to understand the detailed mechanism of action of L-OHP to investigate why L-OHP treatment leads to the upregulation of MYOF. To reiterate, there are still many uncertainties concerning the workings and mechanism of metabolism of L-OHP [29]. Although many studies have reported that L-OHP induces cell death by direct cross-links on nuclear acids as with other platinum-based drugs [29, 30], one recent study documented that L-OHP exerts its cytotoxic action by inducing ribosome biogenesis stress [31], which implies that there are likely some other unknown mechanisms of L-OHP at work. As for the mechanism behind the metabolism of L-OHP, several transporters, such as ABCC1, are thought to be involved in the excretion of L-OHP to the extracellular space [32]. However, there is no solid evidence showing how L-OHP is metabolized into an inactive form. Hence, although additional extensive studies are needed to

elucidate the complete biological mechanism of L-OHP, our findings of a correlation between L-OHP and MYOF could potentially provide a clue leading to a possible solution to understanding the detailed biological mechanism of L-OHP.

In summary, our study highlights the successful establishment of L-OHP-resistant GCOs and detection through microarray analysis of MYOF as a novel gene associated with the L-OHP-based treatment response. We determined that MYOF is highly involved in the susceptibility of GC cells to L-OHP, and its expression is related to tumor progression and unfavorable prognosis in GC patients, especially those receiving platinum-based chemotherapy. In *in vitro* experiments, MYOF KD inhibited cell growth, sphere/organoid formation, migration, and invasion. Our results indicate that MYOF could be a potential biomarker in GC to predict tumor progression and L-OHP sensitivity and also a promising candidate as a novel therapeutic target.

Supplementary Information The online version contains supplementary material available at <https://doi.org/10.1007/s10120-021-01206-4>.

Acknowledgements We thank Mr. Shinichi Norimura (Technical Center, Hiroshima University) for his excellent technical assistance. This research was carried out with the kind cooperation of the Research Center for Molecular Medicine of the Faculty of Medicine of Hiroshima University. We also thank the Analysis Center of Life Science of Hiroshima University for the use of their facilities. The R-spondin-producing cell line was a kind gift from Professor Jeffery Whitsett (Cincinnati Children's Hospital Medical Center, Cincinnati, OH, USA). We would like to thank Professor Eric Fearon (University of Michigan, Ann Arbor, MI, USA) for providing collaborative research resources and comments.

Funding This study was supported by Grants-in-Aid for Scientific Research (JP15H04713, JP16K08691, JP18K07017, JP19H04443) from the Japan Society for the Promotion of Science.

Declarations

Conflict of interest The authors declare that they have no conflict of interest.

References

1. Bray F, Ferlay J, Soerjomataram I, Siegel RL, Torre LA, Jemal A. Global cancer statistics 2018: GLOBOCAN estimates of incidence and mortality worldwide for 36 cancers in 185 countries. *CA Cancer J Clin*. 2018;68:394–424.
2. Holohan C, Van Schaeybroeck S, Longley DB, Johnston PG. Cancer drug resistance: an evolving paradigm. *Nat Rev Cancer*. 2013;13:714–26.
3. Shibue T, Weinberg RA. EMT, CSCs, and drug resistance: the mechanistic link and clinical implications. *Nat Rev Clin Oncol*. 2017;14:611–29.
4. Boj SF, Hwang C-I, Baker LA, Chio II, Engle DD, Corbo V, et al. Organoid models of human and mouse ductal pancreatic cancer. *Cell*. 2015;160:324–38.

5. Lancaster MA, Knoblich JA. Organogenesis in a dish: modeling development and disease using organoid technologies. *Science*. 2014;345:1247125.
6. Seidlitz T, Merker SR, Rothe A, Zakrzewski F, von Neubeck C, Grützmann K, et al. Human gastric cancer modelling using organoids. *Gut*. 2019;68:207–17.
7. Yan HHN, Siu HC, Law S, Ho SL, Yue SSK, Tsui WY, et al. A comprehensive human gastric cancer organoid biobank captures tumor subtype heterogeneity and enables therapeutic screening. *Cell Stem Cell*. 2018;23:882–97.
8. Steele NG, Chakrabarti J, Wang J, Biesiada J, Holokai L, Chang J, et al. An organoid-based preclinical model of human gastric cancer. *Cell Mol Gastroenterol Hepatol*. 2019;7:161–84.
9. van de Wetering M, Francies HE, Francis JM, Bounova G, Iorio F, Pronk A, et al. Prospective derivation of a living organoid biobank of colorectal cancer patients. *Cell*. 2015;161:933–45.
10. Ukai S, Honma R, Sakamoto N, Yamamoto Y, Pham QT, Harada K, et al. Molecular biological analysis of 5-FU-resistant gastric cancer organoids; KHDRBS3 contributes to the attainment of features of cancer stem cell. *Oncogene*. 2020;39:7265–78.
11. Doherty KR, Demonbreun AR, Wallace GQ, Cave A, Posey AD, Heretis K, et al. The endocytic recycling protein EHD2 interacts with myoferlin to regulate myoblast fusion. *J Biol Chem*. 2008;283:20252–60.
12. Bernatchez PN, Sharma A, Kodaman P, Sessa WC. Myoferlin is critical for endocytosis in endothelial cells. *Am J Physiol Cell Physiol*. 2009;297:C484–92.
13. Davis DB, Delmonte AJ, Ly CT, McNally EM. Myoferlin, a candidate gene and potential modifier of muscular dystrophy. *Hum Mol Genet*. 2000;9:217–26.
14. Doherty KR, Cave A, Davis DB, Delmonte AJ, Posey A, Earley JU, et al. Normal myoblast fusion requires myoferlin. *Development*. 2005;132:5565–75.
15. Demonbreun AR, Lapidus KA, Heretis K, Levin S, Dale R, Pytel P, et al. Myoferlin regulation by NFAT in muscle injury, regeneration and repair. *J Cell Sci*. 2010;123:2413–22.
16. Turtoi A, Blomme A, Bellahcène A, Gilles C, Hennequière V, Peixoto P, et al. Myoferlin is a key regulator of EGFR activity in breast cancer. *Cancer Res*. 2013;73:5438–48.
17. Zhang T, Li J, He Y, Yang F, Hao Y, Jin W, et al. A small molecule targeting myoferlin exerts promising anti-tumor effects on breast cancer. *Nat Commun*. 2018;9:3726.
18. Japanese Gastric Cancer Association. Japanese classification of gastric carcinoma: 3rd English edition. *Gastric Cancer*. 2011;14:101–12.
19. Honma R, Goto K, Sakamoto N, Sekino Y, Sentani K, Oue N, et al. Expression and function of Uc. 160+, a transcribed ultraconserved region, in gastric cancer. *Gastric Cancer*. 2017;20:960–9.
20. Sakamoto N, Naito Y, Oue N, Sentani K, Uraoka N, Oo HZ, et al. MicroRNA-148a is downregulated in gastric cancer, targets MMP7, and indicates tumor invasiveness and poor prognosis. *Cancer Sci*. 2014;105:236–43.
21. Saito-Diaz K, Benchabane H, Tiwari A, Tian A, Li B, Thompson JJ, et al. APC inhibits ligand-independent Wnt signaling by the clathrin endocytic pathway. *Dev Cell*. 2018;44:566–81.e8.
22. Sekino Y, Sakamoto N, Goto K, Honma R, Shigematsu Y, Sentani K, et al. Transcribed ultraconserved region Uc. 63+ promotes resistance to docetaxel through regulation of androgen receptor signaling in prostate cancer. *Oncotarget*. 2017;8:94259–70.
23. Sakamoto N, Oue N, Sentani K, Anami K, Uraoka N, Naito Y, et al. Liver-intestine cadherin induction by epidermal growth factor receptor is associated with intestinal differentiation of gastric cancer. *Cancer Sci*. 2012;103:1744–50.
24. Sato T, Vries RG, Snippert HJ, van de Wetering M, Barker N, Stange DE, et al. Single Lgr5 stem cells build crypt-villus structures in vitro without a mesenchymal niche. *Nature*. 2009;459:262–5.
25. Lin L, Li X, Pan C, Lin W, Shao R, Liu Y, et al. ATXN2L upregulated by epidermal growth factor promotes gastric cancer cell invasiveness and oxaliplatin resistance. *Cell Death Dis*. 2019;10:1–13.
26. Wen Q, Chen Z, Chen Z, Chen J, Wang R, Huang C, et al. EphA2 affects the sensitivity of oxaliplatin by inducing EMT in oxaliplatin-resistant gastric cancer cells. *Oncotarget*. 2017;8:47998–8011.
27. Blomme A, Costanza B, de Tullio P, Thiry M, Van Simaey G, Boutry S, et al. Myoferlin regulates cellular lipid metabolism and promotes metastases in triple-negative breast cancer. *Oncogene*. 2017;36:2116–30.
28. Zhang W, Zhou P, Meng A, Zhang R, Zhou Y. Down-regulating myoferlin inhibits the vasculogenic mimicry of melanoma via decreasing MMP-2 and inducing mesenchymal-to-epithelial transition. *J Cell Mol Med*. 2018;22:1743–54.
29. Martínez-Balibrea E, Martínez-Cardús A, Ginés A, Ruiz de Porras V, Moutinho C, Layos L, et al. Tumor-related molecular mechanisms of oxaliplatin resistance. *Mol Cancer Ther*. 2015;14:1767–76.
30. Woynarowski JM, Faivre S, Herzig MC, Arnett B, Chapman WG, Trevino AV, et al. Oxaliplatin-induced damage of cellular DNA. *Mol Pharmacol*. 2000;58:920–7.
31. Bruno PM, Liu Y, Park GY, Murai J, Koch CE, Eisen TJ, et al. A subset of platinum-containing chemotherapeutic agents kills cells by inducing ribosome biogenesis stress. *Nat Med*. 2017;23:461–71.
32. Beretta GL, Benedetti V, Cossa G, Assaraf YG, Bram E, Gatti L, et al. Increased levels and defective glycosylation of MRPs in ovarian carcinoma cells resistant to oxaliplatin. *Biochem Pharmacol*. 2010;79:1108–17.

Publisher's Note Springer Nature remains neutral with regard to jurisdictional claims in published maps and institutional affiliations.